International Journal of Computational and Experimental Science and ENgineering (IJCESEN)

Vol. 11-No.1 (2025) pp. 440-448
http://www.ijcesen.com

ISSN: 2149-9144

Research Article

Material selection and performance analysis of RF-MEMS switch for MM-WAVE applications

R. Karthick[1*], S.P.K. Babu[2], B. Balaji[3]

[1]Department of Physics, Periyar Maniammai Institute of Science and Technology, Thanjavur, Tamilnadu, India
* **Corresponding Author Email:** iamrkarthick85@gmail.com - **ORCID:** 0000-0003-2891-9847

[2]Department of Electronics and Communication Engineering, Periyar Maniammai Institute of Science and Technology, Thanjavur, Tamilnadu, India
Email: spkbabu@pmu.edu - **ORCID:** 0000-0003-2719-9737

[3]Department of Electrical and Electronics Engineering, Periyar Maniammai Institute of Science and Technology, Thanjavur, Tamilnadu, India
Email: mail2krishbala@pmu.edu - **ORCID:** 009-0007-7349-3802

Article Info:

DOI: 10.22399/ijcesen.737
Received : 07 October 2024
Accepted : 19 December 2024

Keywords :

RF-MEMS switch,
mm-wave,
5G communication,
Shunt-Capacitive switch,
Material selection.

Abstract:

This paper presents the design, simulation, and investigation of a fundamental structure for capacitive MEMS switches in a shunt configuration. The main objective is to select materials that achieve low actuation voltage while maintaining RF and dynamic performance, especially for mm-wave applications. The proposed design consists of a Fixed-Fixed flexure beam with dimensions of 260 µm in length, 100 µm in width, and 0.5 µm in thickness. Considering the impact of squeeze film, 60 holes are integrated into the beam membrane, each measuring 64 µm² (8µm x 8µm), and a final gap of 1.9 µm is implemented. The suitability of materials for the beam membrane and dielectric layer in capacitive MEMS switches has been thoroughly examined through a combination of theoretical analysis and software simulations. Aluminum (Al) has emerged as the ideal choice for the beam membrane in mm-wave applications. This preference is defensible by its simulated results to offer a low pull-in voltage of 4V, a quality factor of 1.18, and a switching time of 67 microseconds. Similarly, Si3N4 has been identified as appropriate material, offering a upstate capacitance of 91fF and a downstate capacitance of 7.1pF.

1. Introduction

The millimeter-wave band, typically spanning from 30 GHz to 300 GHz has gathered increasing significance across diverse applications due to its distinct characteristics [1]. Their primary application in 5G cellular networks, where its frequencies facilitate significantly elevated data rates, helps in achieving faster and more efficient communication for developing technologies[2]. 5G networks make use of mm-wave frequencies for their potential to handle higher number of connected devices simultaneously. By implementing technologies such as MIMO (Multiple Input, Multiple Output) and efficient spectrum utilization, 5G systems are aimed to accommodate the demands of the modern age, supporting a multitude of Internet of Things (IoT) devices[3,4].

RF MEMS switches adopt a strategic part for ensuring consistent connectivity and maximizing the overall efficiency of the 5G network by providing the adaptability to operate across a spectrum of frequency bands[5]. The high isolation and low insertion loss, offered by the RF MEMS switches ensures the prevention of signal leakage, safeguards signal strength thereby preserving the reliability and performance of 5G devices[6]. Thus, RF MEMS switches constitute integral part of the 5G ecosystem, providing the necessary flexibility, speed, and competence to navigate between diverse frequency bands and support the demands of modern communication systems.

RF MEMS switches have proved greater effectiveness than conventional mechanical and semiconductor switches, particularly in millimeter-wave frequency range [7,8].

The ohmic contact type are resistive coupled, encounters issues related to excessive current flow, resulting in a shortened switch lifespan and weakened reliability[9]. In contrast, despite comparable power handling capabilities, capacitive contact type switches are preferred for high-frequency applications, such as 5G and potential 6G, due to their superior capacitance ratio between ON and OFF states[10].RF MEMS switches employ various actuation mechanisms, such as thermal, electromagnetic, piezoelectric, and electrostatic methods. Even though the electrostatic mechanism requires higher actuation voltages, its extensive implementation is acceptable by its lower power consumption and favourable linearity [11,12].

The series configuration, incorporating a cantilever structure, achieves higher switching speeds and lower actuation voltages but is suitable for lower frequencies.In contrast, the shunt type with a fixed-fixed structure proves more suitable for high-frequency applications, better stability, simplified fabrication, improved stress management capability, and minimized parasitic effects in continuous transmission lines[13].

Section 2 of the manuscript explains the operational mechanisms and configurations characteristic in the examined design. In Section 3, a detailed analysis of the essential theoretical foundations governing switch design is furnished, covering critical aspects such as switching time, pull-in voltage, and capacitance analysis. Section 4 delivers a detailed explanation of the methodology applied in material selection. Following this, Section 5 explore the results derived from simulations. Section 6 summarises the study's findings and outlines prospects for future exploration.

Design And Working

The switch configuration discussed employs a shunt capacitive bridge with a fixed-fixed beam structure. In its initial state, the beam remains uncontacted, enabling signal flow through the CPW, representing the ON state. Actuation potential induces an electrostatic force, resisted by the mechanical stiffness of the beam. When the pull-in voltage is reached, the electrostatic force surpasses the mechanical restoring force, resulting in the beam snapping down and establishing contact with the central signal line of the CPW. This transition puts the switch in the OFF state, terminating signal flow and connecting the signal to the ground lines. Once actuated, the switch effectively isolates the central signal line.

Upon removal of the applied actuation voltage, the mechanical stiffness of the beam facilitates its return to its original position. Consequently, the switch reverts to its initial state, enabling signal flow through the central signal line to be resumed.

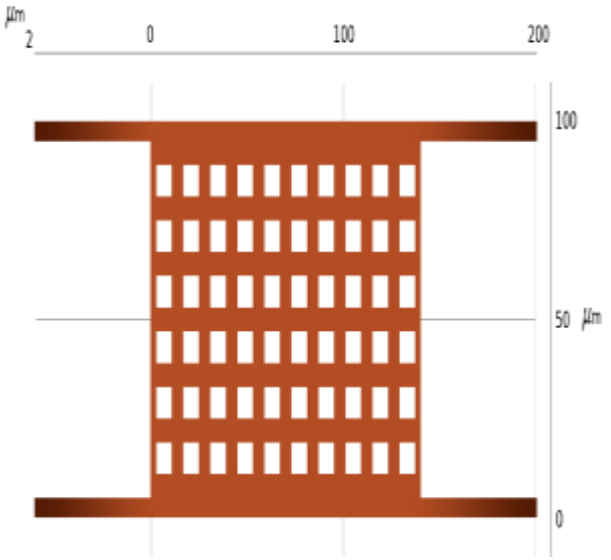

Figure 1. *Top View of beam membrane*

The proposed RF MEMS switch uses 500 µm thick silicon as substrate, covered by a oxide layer of 0.1 µm thickness. The signal line of coplanar waveguide (CPW) with 50Ω impedance is coated with 0.1 µm thick dielectric layer to enhance the switch's RF performance and reliability. Figure 1 illustrates the beam structure, whose spring constant (k) can be determined using the formula provided in Equation (1) [14].

$$k = 4Ew\left(\frac{t}{l}\right)^3 \quad (1)$$

Where, E denotes Young's modulus of the beam, w denotes the width of the beam, and t and l represent the thickness and length of the beam, respectively.

2. Material and Methods

2.1 Theoretical Analysis

Pull-in Voltage

The spring constant of the beam membrane plays a critical role in switch's mechanical operations and in the computation of the pull-down voltage (V_p) given by Equation (2)[15].

$$V_p = V(2g_0/3) = \sqrt{\frac{8k}{27\varepsilon_0 Ww}{g_0}^3} \quad (2)$$

Equation (2) represents the relationship between the pull-down voltage (V_p), the spring constant (k), and the initial gap (g_0). The pull-in voltage decreases proportionally when either k or g_0 is reduced [16].

Switching and release time

An The switching time of an RF MEMS switch is the duration necessary for the downward movement of the bridge membrane to descend and contact the dielectric layer during actuation[17]. Equation (3) governs the determination of switching time (t_s) switch's release time t_r.

$$t_s = 3.67\frac{V_p}{V_s\,\omega_0}\ ;\ t_r = \frac{\pi}{2}\sqrt{\frac{m}{k}} \qquad (3)$$

Where, V_s denotes the supply voltage, and ω_0 (where $\omega_0 = \sqrt{k/m}$)represents the beam's resonant frequency.

2.1.3 Capacitance and RF performance

A well-designed capacitive switch delivers efficient isolation in the downstate while minimizing insertion loss in the upstate. The relationship between upstate and downstate capacitance governs the magnitude of both insertion and isolation losses. Equation (4) represents the ratio of capacitance (C_r) between the upstate and the downstate [18].

$$C_r = \frac{C_d}{C_u} = \frac{\left(\frac{\varepsilon_0\,\varepsilon_r A}{t_d}\right)}{\left(\frac{\varepsilon_0\,A}{g + \frac{t_d}{\varepsilon_r}}\right)} \qquad (4)$$

Where, C_u represents the upstate capacitance, C_d is the downstate capacitance, $t_d$is the dielectric layer's thickness, ε_r denotes the dielectric constant, and ε_0 accounts for the reduction in capacitance due to the roughness of the dielectric-metal interface.

2.2 Material Selection

Material for bridge membrane

Optimizing essential characteristics including pull-in voltage, residual stress, and RF loss involves carefully selecting materials for the switch membrane[19]. Figure 2 (a) and (b) depicts the variations in Poisson's ratio with thermal expansion coefficient and electrical resistivity with thermal conductivity concerning Young's modulus for the various materials recommended for beam design [20-22].

Pull-in voltage

The pulldown of the bridge membrane requires a designated voltage, and optimizing the design is essential to reduce this pull-in voltage requirement. From equations (1) and (2) it is inferred that, to

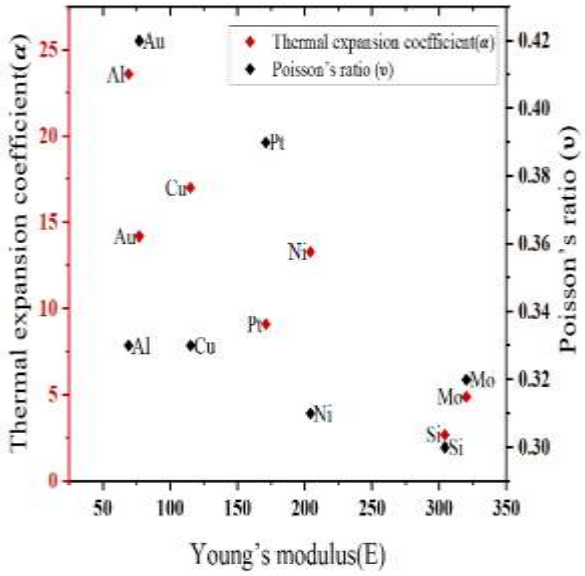

Figure 2. (a) *Comparison of Poisson's ratio and Thermal expansion coefficient with Young's modulus[23]*

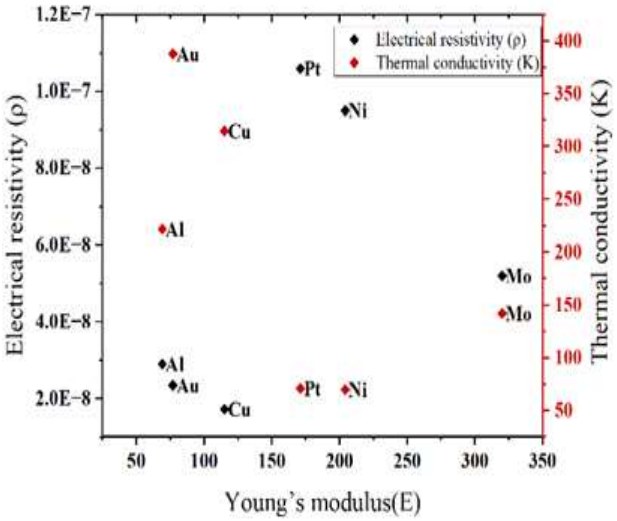

Figure 2. (b) *Comparison of Electrical resistivity and Thermal conductivity with Young's modulus[24]*

effectively reduce the pull-in voltage, select a material with lower Young's modulus[21]. When accounting for residual stress, the spring constant is expressed by Equation (5).

$$\mathrm{K} = \frac{8\gamma(1-\upsilon)(\sigma_0 - \Delta\sigma)tw}{L} \qquad (5)$$

Where, γ is the geometric factor,υ denotes Poisson's ratio, σ_0 indicates initial residual stress, $\Delta\sigma$ represents variation in residual stress. The relationship between the variation in residual stress ($\Delta\sigma$) and temperature is defined by Equation (6).

$$\Delta\sigma = \mathrm{E}\Delta\boldsymbol{\alpha}\Delta T \qquad (6)$$

Where, ΔT denotes change of temperature in the membrane material and Δα represents difference in the thermal expansion coefficient between the membrane and substrate[22]. From equations (5) and (6) it can be inferred that material with a higher Poisson's ratio and thermal expansion coefficient will support to reduce the spring constant of the beam membrane.

RF losses and resistivity

When the RF signal traverses through the membrane, Equation (7) expresses a notable power loss as a result of dissipation,

$$P_{loss} = I^2R \tag{7}$$

Where I represents the current flowing through the beam, and R denotes the resistance of the bridge membrane given by Equation (8).

$$R = \frac{\rho\beta L}{4tw} \tag{8}$$

The constant β reflects current accumulation in the membrane, whereas ρ denotes the material's resistance. Adopting of a low resistivity material for the bridge membrane is a viable approach to lower power loss.

Thermal effects due to RF signal

When the device is exposed to high levels of RF signals, it produces a significant amount of heat, impacting the stability of the switch.

The primary adverse effect resulting from the self-heating of the switch is the occurrence of thermal residual stress, as expressed by Equation (9).

$$\Delta\sigma = E\Delta\alpha\, P_{loss} R_{TH} \tag{9}$$

The self-heating experienced in the system can be calculated by multiplying the electrical resistivity (R) and thermal resistivity R_{TH} of the bridge material, given by Equation (10).

$$R \times R_{TH} = \frac{1}{K}\rho \tag{10}$$

According to Equation (10), undesired thermal effects can be mitigated by using materials with high thermal conductivity and low resistivity values.

Material for dielectric layer

Selecting an appropriate dielectric material characterized by specific properties shows promise in augmenting switch performance without undesirable effects on other relevant parameters.

Figure 3 (a) and (b) depicts the variations in Young's modulus, Thermal expansion coefficient, electrical resistivity and thermal conductivity concerning the dielectric constant for the various materials proposed for the dielectric layer.

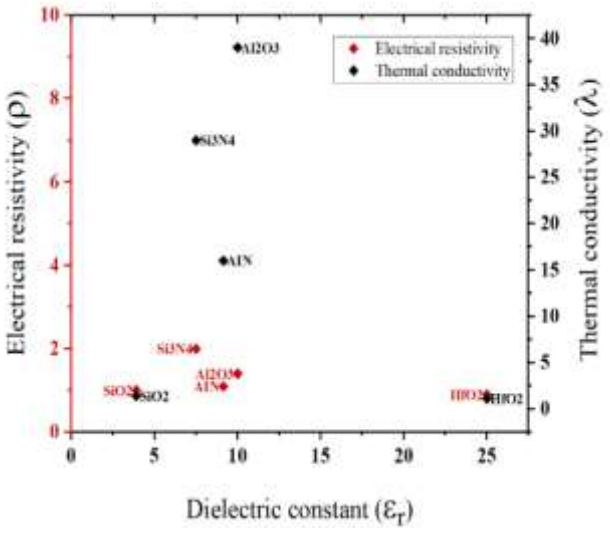

Figure 3. (a) *Analogy of Thermal conductivity and Electrical resistivity with Dielectric constant[23,24]*

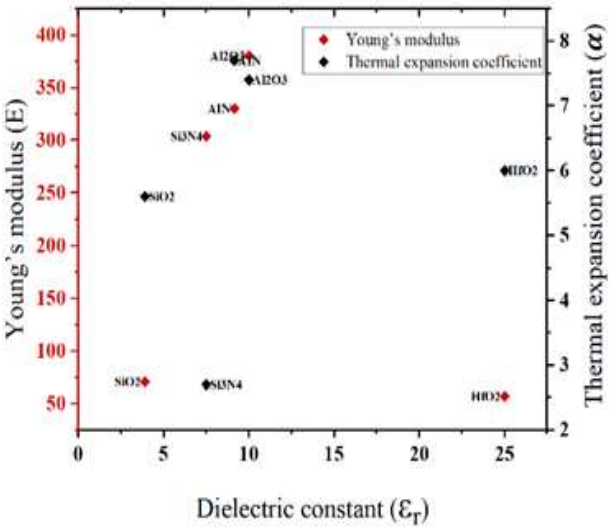

Figure 3. (b) *Analogy of Thermal expansion coefficient and Young's modulus with Dielectric constant*

Charging of dielectric layer

When the actuation voltage is applied, dielectric charging induces stiction between the beam membrane and the dielectric layer, affecting the device's reliability [25]. Equation (11) expresses the decay of polarization after removing the actuation voltage.

$$P(t) = P_p * \exp\left(\frac{-t}{\tau}\right) \tag{11}$$

Where, Pp denotes Steady state Polarization, t represents electrical discharge time and τ is the

Stiction relaxation time which is given by the product electrical resistivity of (ρ) and dielectric constant(ε_r). Equation (11), concluds that the utilization of a dielectric material with high electrical resistivity and dielectric constant contributes to an increased stiction relaxation time. This expedited decay of polarization serves to alleviate the effects of dielectric charging.

Hold –on voltage

When capacitive-type switches are actuated to snap down the bridge membrane, a hold-down voltage is imperative to maintain the beam layer in the down state for a specified duration as described by Equation (12).

$$V_h = \sqrt{\frac{2K}{\varepsilon\varepsilon_0 A}(g_0 - g)\left(g + \frac{t_d}{\varepsilon_r}\right)} \quad (12)$$

Where, V_h represents hold down voltage and g represents overall gap which is the sum of dielectric thickness and air gap (g_0+t_d). Equation (12) shows that a lower hold-down voltage can be achieved by adopting a dielectric material with a high dielectric constant.

Stability of dielectric layer

Reliability of an RF MEMS switch can be figured out by its ability to withstand extended operational cycles, which is quantified by parameters such as dielectric rigidity given by Equation (13) and dielectric breakdown represented by Equation (14) [26].

$$G = \frac{E}{2(1+\upsilon)} \quad (13)$$

$$\Delta\sigma = E\alpha\,\Delta T \quad (14)$$

Based on Equation 13 and 14, it can be inferred that achieving a sensible stability in the dielectric layer necessitates the choice of material with a significant Young's modulus (neither excessively low nor high), lower thermal expansion coefficient and low value for Poisson's ratio [27].

3. Results and Discussions

3.1 Material İmpact on Bridge Membrane

Spring constant and pull-in voltage

Pull-in voltage is a critical factor when customizing the switch for millimeter-wave applications. Figure 4 depicts how the suggested structure responds to spring constant and pull-in voltage across various materials with varying Young's modulus values. The switch membrane was designed and simulated using the Finite Element Method (FEM) software tool COMSOL Multiphysics (version 5.6) with aluminum as beam material, achieving a displacement of 1.9 µm.

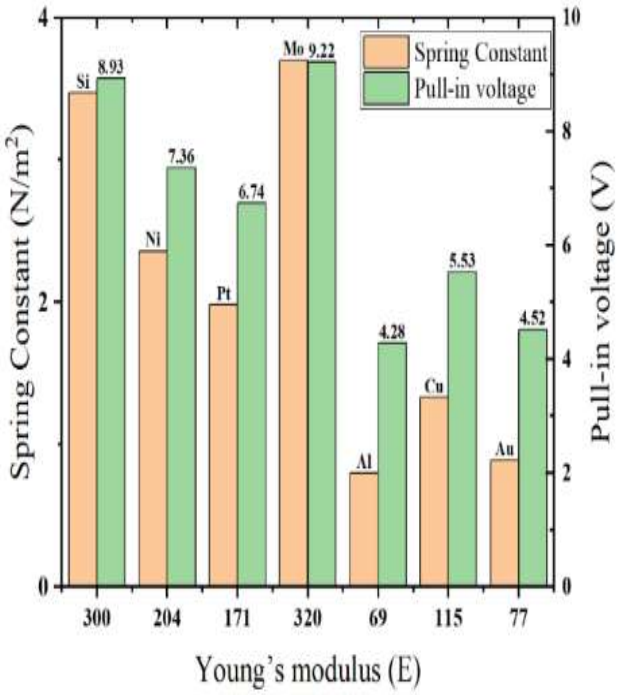

Figure 4. *Pull-in voltage and spring constant response of proposed design across different materials.*

Figure 5 presents the outcomes of the analysis, indicating that Aluminum, possessing a Young's modulus of 69 GPa in the designated structure, exhibits a reduced spring constant of 0.80 N/m^2 with a low pull-in voltage of 4.45 V.

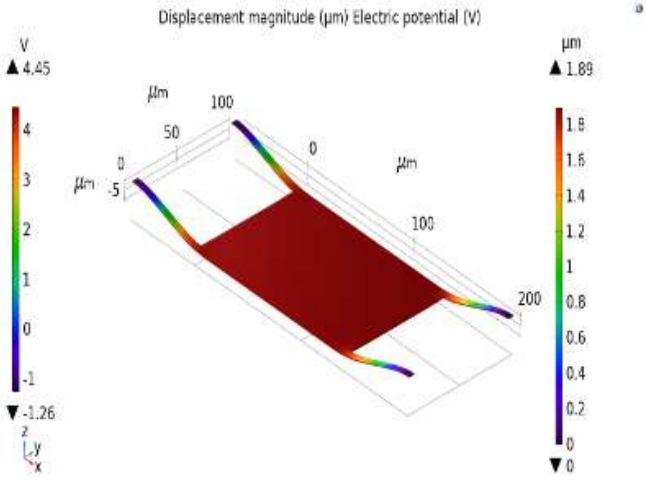

Figure 5. *Pull-in voltage and displacement response of proposed design with aluminum as beam material.*

Resonant frequency

Resonant frequency holds significance in determining key switch parameters like switching time and quality factor. Figure 6 depicts the

discrepancy in resonant frequency response concerning the density of different beam materials for the proposed beam structure.

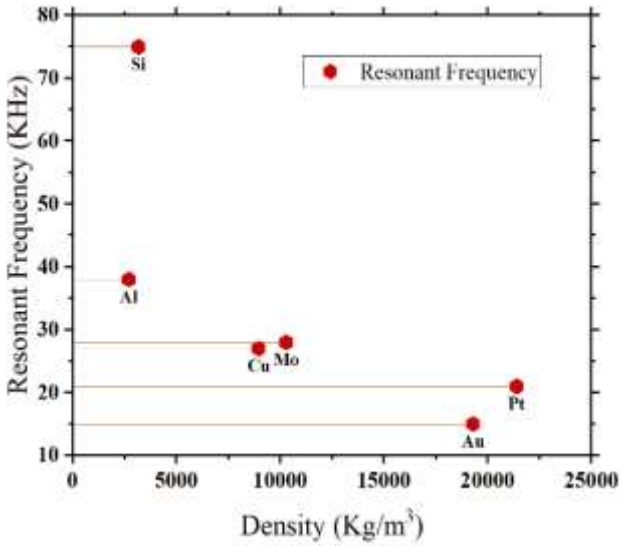

Figure 6. *Density and Resonant frequency response of the proposed structure with different beam materials.*

Quality factor

The beam membrane of the switch is improved by integrating a set of 60 perforations, each measuring 64 µm² (8µm x 8µm). This enhancement is intended to minimize squeeze film damping, reduce pull-in voltage, and enhance switching dynamics.

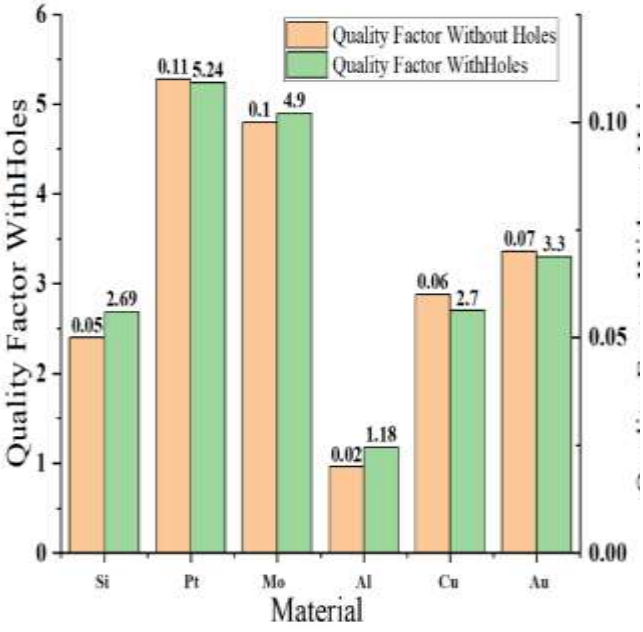

Figure 7. *Change in Quality Factor response as a function of spring constant for various beam materials in the proposed beam structure.*

Figure 7 depicts the change in Quality Factor response about the spring constant of various beam materials for the proposed beam structure, with and without holes. Additionally, the beam structure utilizing aluminum as the beam material exhibits a superior quality factor, expected to be around 1. The simulated results shown in Figure 8 indicate the presence of perforations reduces pull-in voltage from 4.45V to 4V. Moreover, it is deduced from Figure 9 that the inclusion of perforations also aids in stress release.

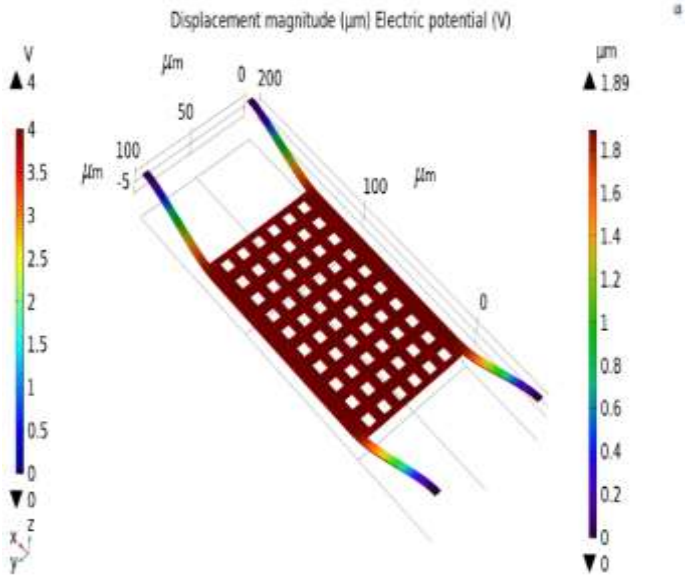

Figure 8. *Response of Displacement and Pull-in Voltage for the Proposed Structure with holes*

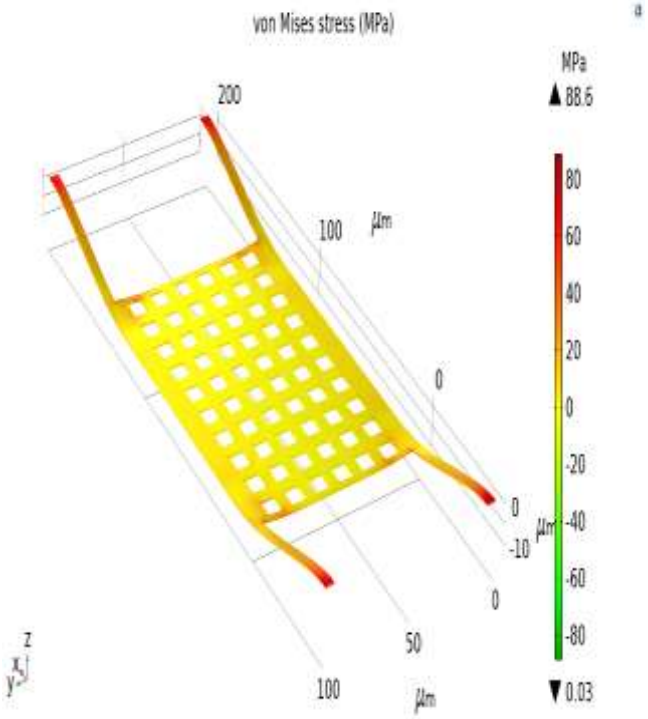

Figure 9. *von Mises stress of the proposed structure made of Al with holes.*

Switching time

Table 1 illustrates the switching time and release time of the beam membrane for the proposed design

employing different materials. Despite the superior performance of Si_3N_4, aluminum is favored over Si_3N_4 due to its advantageous low pull-in voltage.

Table 1. *Switching time and release time of proposed beam membrane*

Material	Switching time (μs)	Release time(μs)
Silicon Nitride	34	3
Nickel	715	68
Platinum	121	11
Molybdenum	61	5.8
Aluminium	67	6
Copper	95	9
Gold	171	16
Silicon Nitride	34	3

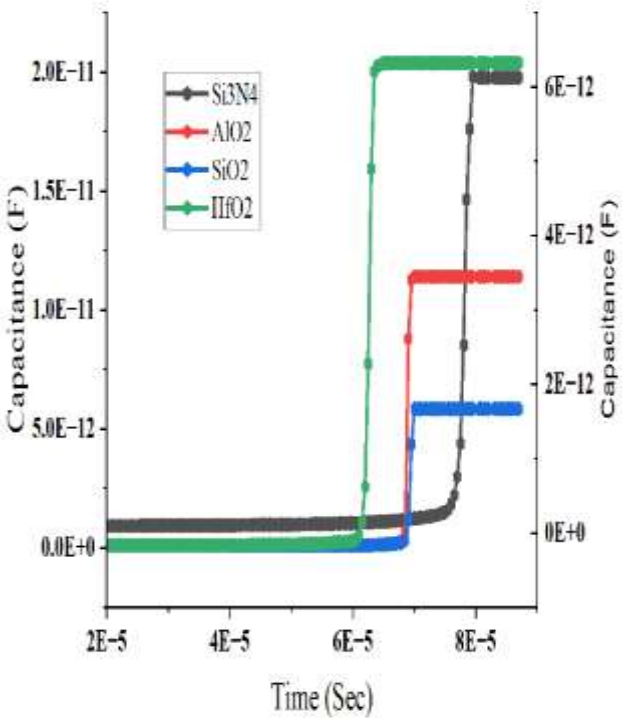

Figure 10. *Capacitance variation Vs Switching time for different dielectric material of the proposed structure*.

3.2 Material impact on dielectric layer

Equation (4) underscores the importance of improving RF performance necessitates increasing the capacitance ratio, which is achieved by using a thin dielectric layer of high dielectric constant. On the other hand, depositing a dielectric layer thinner than 1000 Å presents problems, including pinhole formation and manufacturing complications. Figure 10 illustrates the variation in capacitance of the proposed structure for different dielectric materials concerning switching time. Figures 11 and 12 display the simulated capacitance outcomes of the designed switch in the up-state and down-state respectively, utilizing Si3N4 as the dielectric.

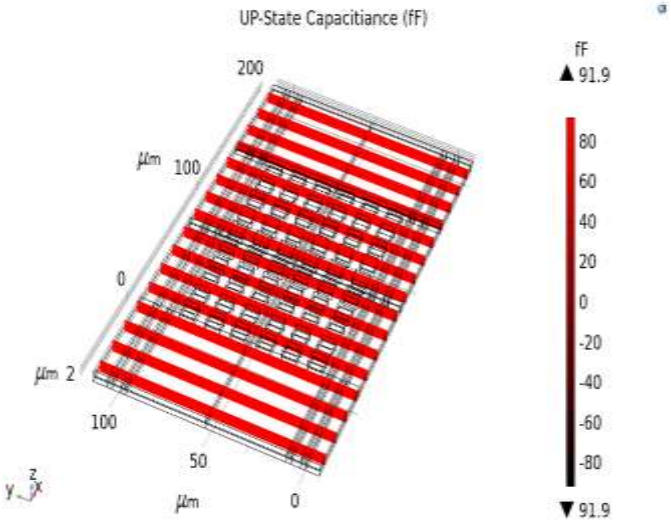

Figure 11. *Capacitance in up state with Si_3N_4 as dielectric layer.*

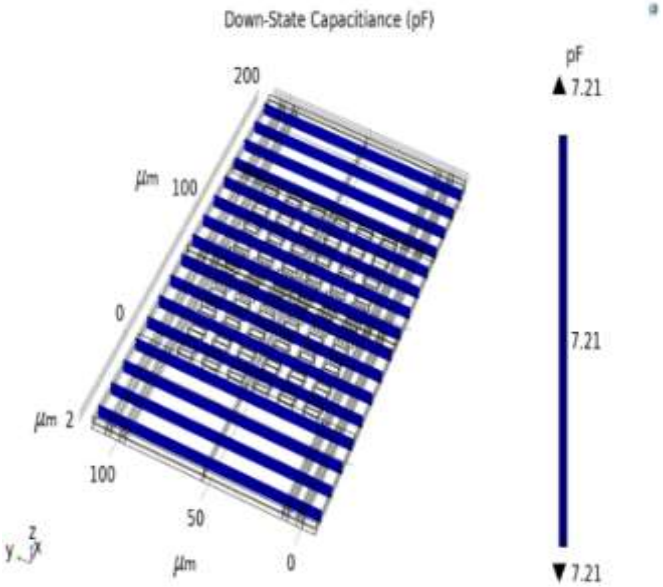

Figure 12. *Capacitance in down state with Si_3N_4 as dielectric layer.*

4. Conclusions

A Fixed-Fixed meandered capacitive shunt MEMS switch has been designed, simulated, and analyzed using various materials to develop MEMS switches suitable for mm-wave applications. The proposed physical structure comprises a beam with dimensions of length 260 μm, width 100 μm, and thickness 0.5 μm. It incorporates a Fixed-Fixed flexure design. Additionally, 60 holes are integrated into the beam membrane, each measuring 64 μm² (8μm x 8μm), with a gap of 1.9 μm. The analysis conducted on beam materials indicates that Aluminum (Al) surpasses other materials, showcasing superior performance with 0.80 N/m² of spring constant, resonant frequency of 38KHz, low

pull-in voltage of 4V, switching time of 67 µs with a quality factor of 1.18. Conversely, Si_3N_4 demonstrates superior capacitance values, with 91fF of up-state capacitance and 7.1pF of down-state capacitance. The future scope of this work involves implementing serpentine meanders to reduce the pull-in voltage and switching time further. Similar works were done and reported in the literature [28-42].

Author Statements:

- **Ethical approval:** The conducted research is not related to either human or animal use.
- **Conflict of interest:** The authors declare that they have no known competing financial interests or personal relationships that could have appeared to influence the work reported in this paper
- **Acknowledgement:** The authors declare that they have nobody or no-company to acknowledge.
- **Author contributions:** The authors declare that they have equal right on this paper.
- **Funding information:** The authors declare that there is no funding to be acknowledged.
- **Data availability statement:** The data that support the findings of this study are available on request from the corresponding author. The data are not publicly available due to privacy or ethical restrictions.

References

[1] Kurmendra and R. Kumar. (2021). A review on RF micro-electro-mechanical-systems (MEMS) switch for radio frequency applications. *Microsyst. Technol.*, 27(7):2525–2542. doi: 10.1007/s00542-020-05025-y.

[2] A. Tkachenko, I. Lysenko, and A. Kovalev. (2023). Investigation and Research of High-Performance RF MEMS Switches for Use in the 5G RF Front-End Modules. *Micromachines*. 14(2):477. doi: 10.3390/mi14020477.

[3] J. Casals-Terré et al. (2022). Enhanced Robustness of a Bridge-Type Rf-Mems Switch for Enabling Applications in 5G and 6G Communications. *Sensors*. 22(22):8893. doi: 10.3390/s22228893.

[4] K. Joy, A. Swarnkar, M. S. Giridhar, A. DasGupta, and D. R. Nair. (2023). RF MEMS capacitive shunt switch for low loss applications. *J. Micromechanics Microengineering*. 33(3):034004. doi: 10.1088/1361-6439/acb58c.

[5] X. You et al. (2021). Towards 6G wireless communication networks: vision, enabling technologies, and new paradigm shifts. *Sci. China Inf. Sci.* 64(1):110301. doi: 10.1007/s11432-020-2955-6.

[6] T. Cao, T. Hu, and Y. Zhao. (2020). Research Status and Development Trend of MEMS Switches: A Review. *Micromachines.* 11(7):694. doi: 10.3390/mi11070694.

[7] R. Karthick and S. P. K. Babu. (2020). Review on Radio Frequency Micro Electro Mechanical Systems (RF-MEMS). *Switch.* 637. doi: 10.1007/978-981-15-2612-1_43.

[8] D. Dubuc, K. Grenier, and J. Iannacci. (2022). RF-MEMS for smart communication systems and future 5G applications. *Smart Sensors MEMs.* 499–539. doi: 10.1016/B978-0-08-102055-5.00018-8.

[9] J. Iannacci and H. V. Poor. (2022). Review and Perspectives of Micro/Nano Technologies as Key-Enablers of 6G. *IEEE Access.*10:55428–55458. doi: 10.1109/ACCESS.2022.3176348.

[10] N. Zhang, Z. Yan, R. Song, C. Wang, Q. Guo, and J. Yang. (2019). Design and Performance of a J Band MEMS Switch. *Micromachines.*10(7):467. doi: 10.3390/mi10070467.

[11] S. P. Chokkara, A. Gaur, K. G. Sravani, B. Balaji, and K. S. Rao. (2022). Design, Simulation and Analysis of a Slotted RF MEMS Switch. *Trans. Electr. Electron. Mater.* 23(4):419–429. doi: 10.1007/s42341-021-00363-8.

[12] A. Kashani Ilkhechi, H. Mirzajani, E. Najafi Aghdam, and H. Badri Ghavifekr. (2017). A new electrostatically actuated rotary three-state DC-contact RF MEMS switch for antenna switch applications. *Microsyst. Technol.*23(1):231–243. doi: 10.1007/s00542-015-2714-1.

[13] Q. Wu et al. (2023). Design and fabrication of a series contact RF MEMS switch with a novel top electrode. *Nanotechnol. Precis. Eng.* 6(1). doi: 10.1063/10.0016903.

[14] G. M. Rebeiz. (2003). RF MEMS: Theory,Design, and Technology. *Wiley*. doi: 10.1002/0471225282.

[15] Kai Chang. (1994). Microwave Solid-State Circuits and Applications. *Wiley*.

[16] G. M. Rebeiz and J. B. Muldavin. (2001). RF MEMS switches and switch circuits. *IEEE Microw. Mag.* 2(4):59–71. doi: 10.1109/6668.969936.

[17] V. K. Varadan, K. J. Vinoy, and K. A. Jose. (2003). RF MEMS and Their Applications. *Wiley*.

[18] H. Feng, J. Zhao, C. Zhou, and M. Song. (2022). Design and Analysis of the Capacitive RF MEMS Switches with Support Pillars. *Sensors.*22(22). doi: 10.3390/s22228864.

[19] Kurmendra and R. Kumar. (2021). Investigations on beam membrane and dielectric materials using Ashby's methodology and their impact on the performance of a MEMS capacitive switch. *Microsyst. Technol.* 27(12):4269–4289. doi: 10.1007/S00542-021-05220-5.

[20] R. Kumari and M. Angira. (2022). FEM simulation and material selection for enhancing the performance of a RF-MEMS capacitive switch. *Artic. J. Comput. Electron.* doi: 10.1007/s10825-022-01905-w.

[21] G. Guisbiers, E. Herth, B. Legrand, N. Rolland, T. Lasri, and L. Buchaillot. (2010). Materials selection procedure for RF-MEMS. *Microelectron. Eng.* 87(9):1792–1795. doi: 10.1016/j.mee.2009.10.016.

[22] J. G. Noel. (2016). Review of the properties of gold material for MEMS membrane applications. *IET Circuits, Devices Syst.* 10(2):156–161. doi: 10.1049/iet-cds.2015.0094.

[23] M. F. Ashby, Y. J. M. Bréchet, D. Cebon, and L. Salvo. (2004). Selection strategies for materials and processes. *Mater. Des.* 25(1):51–67. doi: 10.1016/S0261-3069(03)00159-6.

[24] Kurmendra and R. Kumar. (2021). Materials Selection Approaches and Fabrication Methods in RF MEMS Switches. *J. Electron. Mater.* 50(6):3149–3168. doi: 10.1007/s11664-021-08817-8.

[25] W. M. van Spengen. (2012). Capacitive RF MEMS switch dielectric charging and reliability: a critical review with recommendations. *J. Micromechanics Microengineering*. 22(7):074001. doi: 10.1088/0960-1317/22/7/074001.

[26] S. Shekhar, K. J. Vinoy, and G. K. Ananthasuresh. (2017). Surface-Micromachined Capacitive RF Switches With Low Actuation Voltage and Steady Contact. *J. Microelectromechanical Syst.* 26(3): 643–652. doi: 10.1109/JMEMS.2017.2688519.

[27] A. Basu, G. G. Adams, and N. E. McGruer. (2016). A review of micro-contact physics, materials, and failure mechanisms in direct-contact RF MEMS switches. *J. Micromechanics Microengineering*. 26(10):104004. doi:10.1088/0960-317/26/10/104004.

[28]Syam Kumar Duggirala, M. Sathya, & Nithya Poupathy. (2025). Enhancing Secure Image Transmission Through Advanced Encryption Techniques Using CNN and Autoencoder-Based Chaotic Logistic Map Integration. *International Journal of Computational and Experimental Science and Engineering*, 11(1). https://doi.org/10.22399/ijcesen.761

[29]Hadi Athab Hamed, & Ahmed Kareem ABDULLAH. (2025). M-ary Pulse Ampplitude Modulation Recognition Using Discrete Meyer Wavelet and Reverse Biorthogonal Wavelet. *International Journal of Computational and Experimental Science and Engineering*, 11(1). https://doi.org/10.22399/ijcesen.749

[30]ONAY, M. Y. (2024). Secrecy Rate Maximization for Symbiotic Radio Network with Relay-Obstacle. *International Journal of Computational and Experimental Science and Engineering*, 10(3). https://doi.org/10.22399/ijcesen.413

[31]MOHAMED, N. N., Yulianta SIREGAR, Nur Arzilawati MD YUNUS, & Fazlina MOHD ALI. (2024). Modelling the Hybrid Security Approach for Secure Data Exchange: A Proof of Concept. *International Journal of Computational and Experimental Science and Engineering*, 10(4). https://doi.org/10.22399/ijcesen.344

[32]Radhi, M., & Tahseen, I. (2024). An Enhancement for Wireless Body Area Network Using Adaptive Algorithms. *International Journal of Computational and Experimental Science and Engineering*, 10(3). https://doi.org/10.22399/ijcesen.409

[33]Iqbal, A., Shaima Qureshi, & Mohammad Ahsan Chishti. (2025). Bringing Context into IoT: Vision and Research Challenges. *International Journal of Computational and Experimental Science and Engineering*, 11(1). https://doi.org/10.22399/ijcesen.760

[34]N. Vidhya, & C. Meenakshi. (2025). Blockchain-Enabled Secure Data Aggregation Routing (BSDAR) Protocol for IoT-Integrated Next-Generation Sensor Networks for Enhanced Security. *International Journal of Computational and Experimental Science and Engineering*, 11(1). https://doi.org/10.22399/ijcesen.722

[35]Kılıçarslan, M. (2024). The Effect of Emotional Intelligence on Social Media Advertising Perception . *International Journal of Computational and Experimental Science and Engineering*, 10(1). https://doi.org/10.22399/ijcesen.293

[36]B. Paulchamy, Vairaprakash Selvaraj, N.M. Indumathi, K. Ananthi, & V.V. Teresa. (2024). Integrating Sentiment Analysis with Learning Analytics for Improved Student. *International Journal of Computational and Experimental Science and Engineering*, 10(4). https://doi.org/10.22399/ijcesen.781

[37]Ganta, S. R., & Naga Malleswara Rao Nallamothu. (2025). A dynamic integrity and data confidentiality based wireless N2N data communication and security protocol on large networks. *International Journal of Computational and Experimental Science and Engineering*, 11(1). https://doi.org/10.22399/ijcesen.720

[38]Robert, N. R., A. Cecil Donald, & K. Suresh. (2025). Artificial Intelligence Technique Based Effective Disaster Recovery Framework to Provide Longer Time Connectivity in Mobile Ad-hoc Networks. *International Journal of Computational and Experimental Science and Engineering*, 11(1). https://doi.org/10.22399/ijcesen.713

[39]Sushma Polasi, & Hara Gopal Venkata Vajjha. (2024). Secure Drone Communications using MQTT protocol. *International Journal of Computational and Experimental Science and Engineering*, 10(4). https://doi.org/10.22399/ijcesen.685

[40]S. Praseetha, & S. Sasipriya. (2024). Adaptive Dual-Layer Resource Allocation for Maximizing Spectral Efficiency in 5G Using Hybrid NOMA-RSMA Techniques. *International Journal of Computational and Experimental Science and Engineering*, 10(4). https://doi.org/10.22399/ijcesen.665

[41]El-Taj, H. (2024). A Secure Fusion: Elliptic Curve Encryption Integrated with LSB Steganography for Hidden Communication. *International Journal of Computational and Experimental Science and Engineering*, 10(3). https://doi.org/10.22399/ijcesen.382

[42]V, V., & S, V. (2024). Double Deep Q- energy aware Service allocation based on Dynamic fractional frequency reusable technique for lifetime maximization in HetNet-LTE network. *International Journal of Computational and Experimental Science and Engineering*, 10(4). https://doi.org/10.22399/ijcesen.543